JOURNAL OF SOLID STATE CHEMISTRY **134,** 67–75 (1997)
ARTICLE NO. SC977537

Adsorption Characteristics of $LaNi_5$ Particles

M. Y. Song[1] and H. R. Park*

Faculty of New Materials Engineering, Chonbuk National University, 664-14 1ga Deogzindong Chonju, Chonbuk, 561-756, Korea, and
** Department of Chemical Technology, Chonnam National University, 300 Yongbongdong Bukgu, Kwangju, 500-757, Korea*

Received February 13, 1996; in revised form June 30, 1997; accepted July 8, 1997

Nitrogen adsorption on an intermetallic compound, $LaNi_5$, was studied before and after activation and after hydriding–dehydriding cycling. The specific surface area of activated $LaNi_5$ was $0.271 \pm 0.004\ m^2\ g^{-1}$. Adsorption and desorption isotherms of activated $LaNi_5$ were obtained. The adsorption isotherm was similar to type II among the five types of isotherms classified by S. Brunauer, L. S. Deming, W S. Deming, and E. Teller (*J. Am. Chem. Soc.* 62, 1723, 1940). Its hysteresis curve had the type B form among de Boer's five types of hysteresis. Desorption pore-size analyses showed that the activated $LaNi_5$ had only a few mesopores, the diameters of which were around 20–110 Å. The average adsorption rate of the activated $LaNi_5$ showed a first-order dependence on nitrogen pressure at 77 K.

INTRODUCTION

$LaNi_5$, FeTi, Mg_2Ni, and AB_2-type Laves phase are well-known hydrogen-storage intermetallic compounds that have been investigated by many researchers (1–15). Among these intermetallic compounds, $LaNi_5$, FeTi, and E_rFe_2, one of the AB_2-type Laves phases, have equilibrium plateau pressures higher than 1 bar even at 273 K, and therefore the heat necessary for hydrogen evolution can be easily provided from the cooling water used for heat exchange.

One of the important steps in the hydriding (dehydriding) reaction is the adsorption (desorption) step on the metal surface. Therefore, it is worthwhile to investigate the surface state of the sample in detail to study the hydriding and dehydriding kinetics.

According to the study of Park and Lee on the hydriding kinetics of $LaNi_5$ (16), the hydriding rate of $LaNi_5$ shows a first-order dependence on hydrogen pressure in the lower range of fractional conversion, and is controlled by the hydrogen adsorption on the particle surface. However, studies of the adsorption characteristics of $LaNi_5$ are few. In this work N_2 BET surface area of $LaNi_5$ was investigated before and after the activation process (for hydriding and dehydriding reactions) and after hydriding–dehydriding cycling; the nitrogen adsorption and desorption isotherms of the activated samples and the dependence of adsorption rate on nitrogen pressure are reported.

[1] To whom correspondence should be addressed.

EXPERIMENTAL

$LaNi_5$ samples were prepared by arc melting under argon atmosphere. The samples were remelted three or four times to improve their homogeneity. They were then annealed under vacuum for 3 days. Samples prepared likewise were crushed into $-100 + 200$ mesh (74–149 μm).

Hydriding and dehydriding reactions were activated in a Sievert-type high-pressure hydriding–dehydriding apparatus made of stainless steel. The samples were hydrided and dehydrided 11 times between 10^{-2} Torr and 20 bar H_2 at room temperature.

A Quantasorb sorption system was used to determine the specific surface areas (surface areas per unit weight) of the $LaNi_5$ sample before and after activation by the technique of adsorbing an adsorbate gas from a flowing mixture of adsorbate and inert nonadsorbable carrier gas. The processes of adsorption and desorption are monitored by measuring the variation in the thermal conductivity of the gas mixture.

Figure 1 is a typical adsorption–desorption cycle. Adsorption was started (A in Fig. 1) by immersing the sample contained in a sample cell into liquid nitrogen. When the gas was adsorbed on the sample surface, the density of the adsorbing gas decreased. It led to a variation in the thermal conductivity of the gas mixture, giving rise to an adsorption peak. When the adsorption was completed, there no longer existed any difference between the thermal conductivities of the gases entering and leaving the sample cell. This situation is indicated by the return of the meter to the baseline. Desorption was initiated at point B (in Fig. 1) by removal of sample from the liquid nitrogen. During the desorption process the gas leaving the sample cell is enriched in the adsorbate. Therefore, the signal is opposite in polarity to

0022-4596/97 $25.00

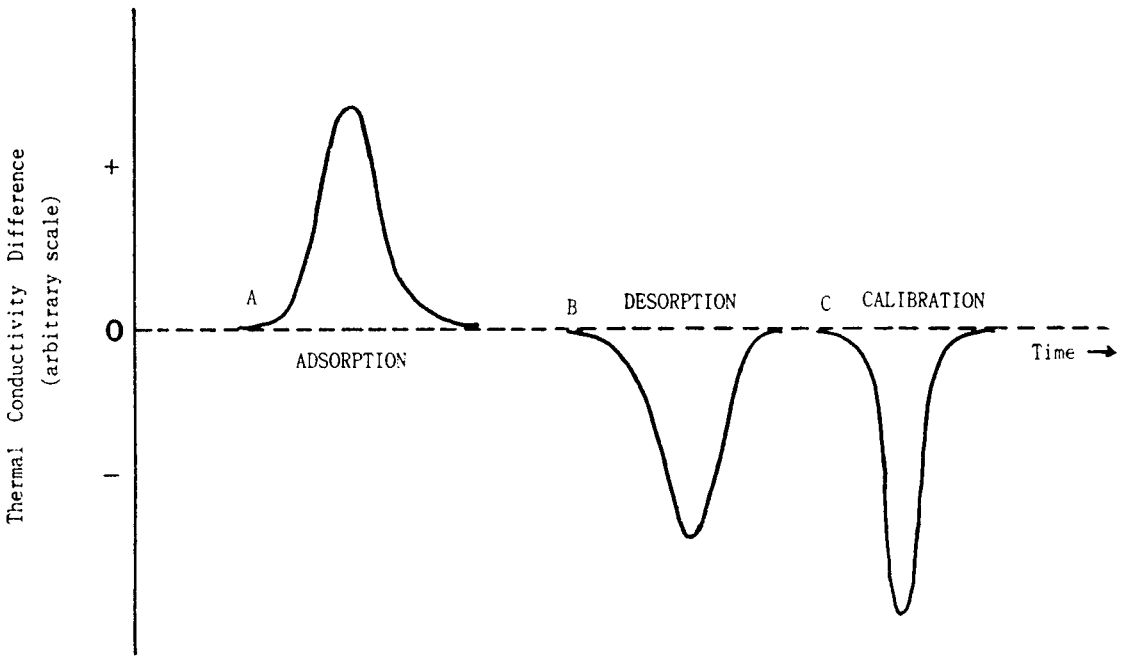

FIG. 1. Adsorption, desorption, and calibration peaks.

that obtained during adsorption. The "DES" and "ADS" switches are used to keep all signals positive. To obtain a sharp desorption peak hot air was blown on the sample cell with a heat gun immediately after removing the sample cell from the liquid nitrogen. Then the sample was immersed into the water at room temperature. This treatment allowed the sample to attain room temperature in a short time. At point C of Fig. 1 a known amount of the adsorbate was introduced into the flow stream to calibrate the desorption signal.

The volume of nitrogen (adsorbate) adsorbed on the sample surface and then desorbed when the cell is warmed is calculated from the equation

$$V_{\text{des}} = V_{\text{cal}} \frac{A_{\text{des}}}{A_{\text{cal}}}, \qquad [1]$$

where V_{des} is the volume of adsorbate desorbed and V_{cal} the calibration volume. A_{des} and A_{cal} are the integrator readings from the signal and the calibration, respectively. The integrator readings are the numbers read from the integrator of the Quantasorb sorption system, which are proportional to the signal areas.

The outgassing before the measurements of surface area and adsorption and desorption isotherms was carried out by the method suggested by Lopez-Gonzales *et al.* (17). The sample was adsorption–desorption cycled six times under a relative pressure $P/P_0 = 0.3$, where P is the partial pressure of adsorbate and P_0 the saturated vapor pressure of the adsorbate. The measured results were quite reproducible after the outgassing process.

For the measurements of the sample surface area adsorption, desorption and calibration peaks were obtained at mole fractions of nitrogen equal to 0.1, 0.2, and 0.3 by the process described above. The results obtained were applied to the BET equation to calculate the surface area.

To obtain the adsorption isotherm, the quantities of adsorbed nitrogen were measured for the various concentrations of nitrogen (10, 20, … , %) in the helium–nitrogen gas mixtures. Then these quantities were plotted as a function of the relative pressure of nitrogen.

For the desorption isotherms, nitrogen of 99% mole fraction was made to flow into the sample cell immersed in the liquid nitrogen, and completion of the adsorption was awaited. Then pure nitrogen was made to flow into the sample cell for 1 or 2 min to saturate the sample surface completely with nitrogen gas. With the sample immersed in the liquid nitrogen, the concentration of the gas mixture was changed, for example, to 90% nitrogen mole fraction. Excess adsorbate would desorb from the sample surface and the sample would be equilibrated with a nitrogen 90% adsorbate gas. By measuring this quantity we obtained the point corresponding to nitrogen 90%. The above process was repeated by varying the concentrations of the gas mixture into nitrogen 80, 70, … , %.

For identification of the $LaNi_5$ phase and observation of the variation in X-ray diffraction pattern with activation,

X-ray diffraction spectra were obtained with Cu$K\alpha$ radiation filtered with Ni for the $LaNi_5$ samples, before and after the activation process. The changes in the microstructure of the samples before and after the activation process were observed by scanning electron microscope.

RESULTS AND DISCUSSION

Figure 2 shows the X-ray diffraction patterns of $LaNi_5$ before and after activation. The peaks of the sample after activation were slightly broadened. This occurs because the particles are finer after activation than before activation.

Figure 3 gives the adsorption, desorption, and calibration peaks of the activated $LaNi_5$ when a conventional sample cell is used. The N_2 mole fraction in the gas mixture was 0.3, the flow rate of the gas mixture 20 $cm^3\,min^{-1}$, and the bridge current 152 mA. The calibration peak corresponds to a calibration volume of 0.33 cm^3 (754 mm Hg, 302 K). For the adsorption and desorption peaks, small initial peaks appear. According to Kourilova and Krevel (18) and Lowell and Karp (19), they result from thermal diffusion. The thermal diffusion causes the adsorption and desorption peaks to separate when the gas mixture is exposed to a changing temperature gradient. The arms of the sample cell undergo an abrupt temperature gradient changing in a short time until steady state, when they enter or leave the liquid nitrogen. This leads heavier molecules to move to higher-temperature regions. This thermal diffusion effect can be eliminated by using a microcell instead of the conventional sample cell used. When a microcell is used, measurements should be made at high bridge current and low attenuation since only a small quantity of the sample can be placed in the sample cell. In this case, the baseline was unstable.

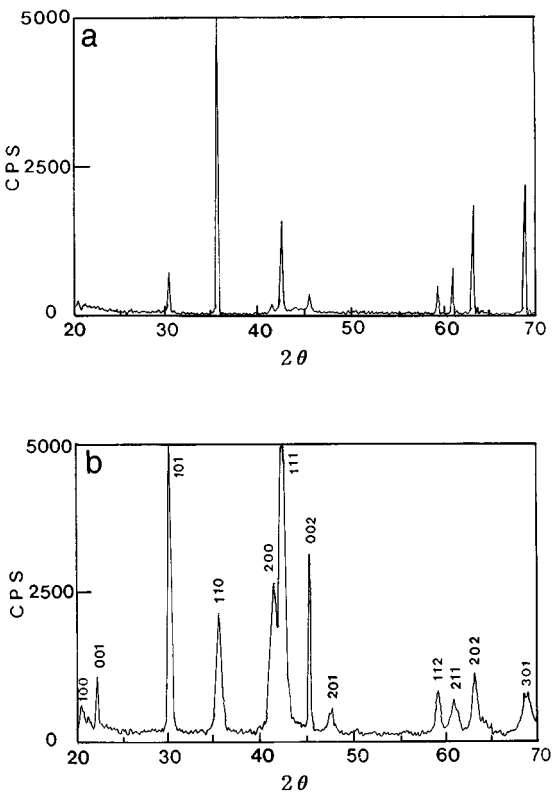

FIG. 2. X-ray powder diffraction patterns of $LaNi_5$ (a) before activation and (b) after activation.

From the determinations of the quantity by desorption we measured the quantity of the absorbed nitrogen and obtained the adsorption and desorption isotherms. Since the desorption peak in Fig. 3 exhibits a very small initial peak resulting from the thermal diffusion effect, we used a conventional sample cell when we measured the surface area of the samples before and after activation and the adsorption and desorption isotherms.

According to BET theory (20),

$$\frac{1}{X[(P_0/P)-1]} = \frac{1}{X_m C} + \frac{C-1}{X_m C}\left(\frac{P}{P_0}\right), \qquad [2]$$

where P is the partial pressure of the adsorbate, P_0 the saturated vapor pressure of the adsorbate, X the weight of the adsorbate adsorbed at a relative pressure P/P_0, X_m the weight of adsorbate adsorbed at a coverage of one monolayer, and C the BET constant, which depends on the heat of the adsorbate condensation and the heat of adsorption.

By applying this BET equation [2], we determine the surface area. The plot of $1/X[(P_0/P)-1]$ versus (P/P_0) usually becomes linear in the range $0.05 \le P/P_0 \le 0.35$.

The slope s and intercept i of the BET equation are given by

$$s = \frac{C-1}{X_m C}, \qquad [3]$$

$$i = \frac{C-1}{X_m C}. \qquad [4]$$

Solving Eqs. [3] and [4] for X_m and C yields

$$X_m = \frac{1}{s+i}, \qquad [5]$$

$$C = \frac{s}{i} + 1. \qquad [6]$$

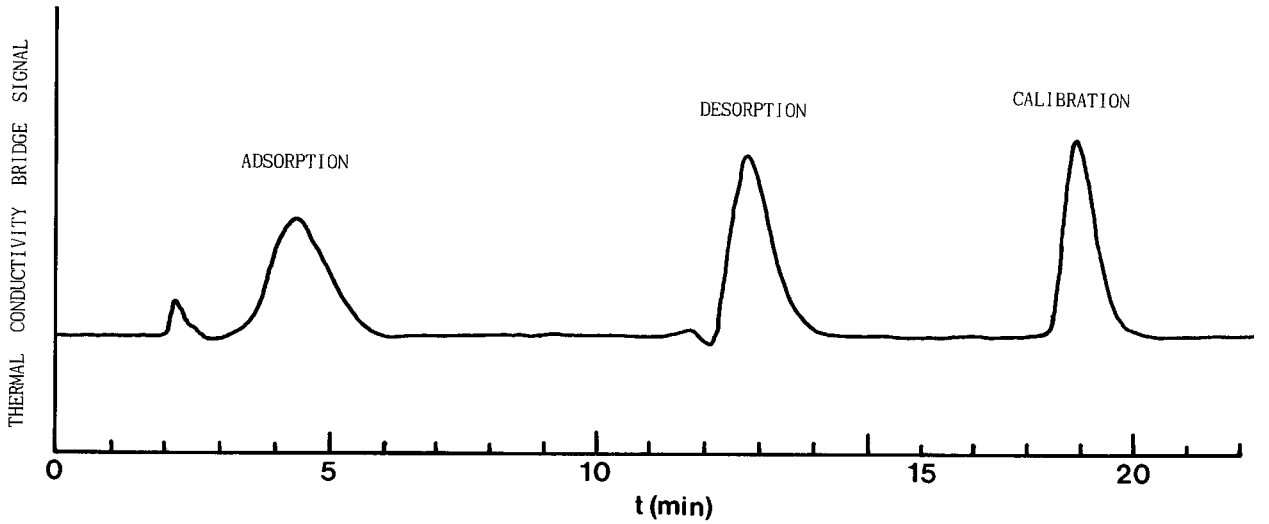

FIG. 3. Adsorption, desorption, and calibration peaks of the activated $LaNi_5$ for N_2 mole fraction = 0.3.

The total surface area of the sample, S_t is determined from

$$S_t = \frac{X_m N_A S_{ad}}{M}, \qquad [7]$$

where N_A is Avogadro's number, M the adsorbate molecular weight, and S_{ad} the cross-sectional area of the adsorbate molecule. The S_{ad} of nitrogen used in this work is $16.2 \times 10^{-20}\,m^2$ (16.2Å^2). This value is calculated from the following equation established by Brunauer, Emmett, and Teller,

$$S_{ad} = 1.091\left(\frac{M}{\rho N_A}\right)^{2/3}, \qquad [8]$$

where ρ is the liquid density of the adsorbate, a factor 1.091 the value calculated from the close-packed hexagonal arrangement of the nitrogen molecule assumed spherical.

The specific surface area, S, is determined by dividing S_t by the sample weight, W:

$$S = S_t/W. \qquad [9]$$

Figure 4a is the BET plot of $LaNi_5$ with particle size $-100 + 200$ mesh (74–149 μm) before activation. The total surface area calculated from this BET plot was 0.189 m^2. The sample weight was 4.30 g, leading to a specific surface area of 0.044 $m^2\,g^{-1}$.

Figure 4b is a BET plot of $LaNi_5$ after activation (at room temperature, 11 hydriding–dehydriding cycles between 0 and 20 bar H_2). The total surface area was calculated as 1.070 m^2. The sample weight was 3.91 g. The specific surface area was found to be 0.274 $m^2\,g^{-1}$ for this BET plot. For this sample the specific surface area was measured 12 times. The average specific surface area was 0.271 $m^2\,g^{-1}$ and its confidence limit was $\pm$ 0.004. The factor (t) for confidence interval of 95% is 2.20 for 12 observations. The specific surface area of 0.271 $\pm$ 0.004 $m^2\,g^{-1}$ agrees reasonably with the values of 0.29 $m^2\,g^{-1}$ found by Tanaka *et al.* (21) and 0.25 $m^2\,g^{-1}$ by van Mal (22). These results show that the specific surface area of $LaNi_5$ after activation was about seven times as large as that before activation.

Particles expand during the hydriding reaction and contract during the dehydriding reaction. The repetition of expansion and contraction with hydriding–dehydriding cycling decreases particle size. This is considered to lead to the increase in specific surface area after activation.

Figure 5 shows the variation of the specific surface area, S, of $LaNi_5$ with the number of hydriding–dehydriding cycles, n. Hydriding–dehydriding cycling was carried out between about 10^{-2} Torr and 8 bar H_2. Specific surface area increased with the increase in n, and after 2530 cycles it was approximately 10 times as large as that before cycling.

In many studies on hydriding–dehydriding kinetics, it has been assumed that the specific surface area does not vary with the number of cycles and remains constant. Our results show that this assumption is not reasonable. The increase in the number of hydriding–dehydriding cycles is unavoidable during the experiment for the kinetic study. To reduce the effect of the increase in specific surface area with cycling, the kinetic data must be obtained and analyzed in a range of n as narrow as possible.

Table 1 gives the variation of the specific surface areas, S ($m^2\,g^{-1}$), of $LaNi_5$ with the number of the hydriding–dehydriding cycles, n.

Figure 6 shows the adsorption and desorption isotherms, plots of V^{STP} versus P/P_0, where V^{STP} ($cm^3\,g^{-1}$) is the

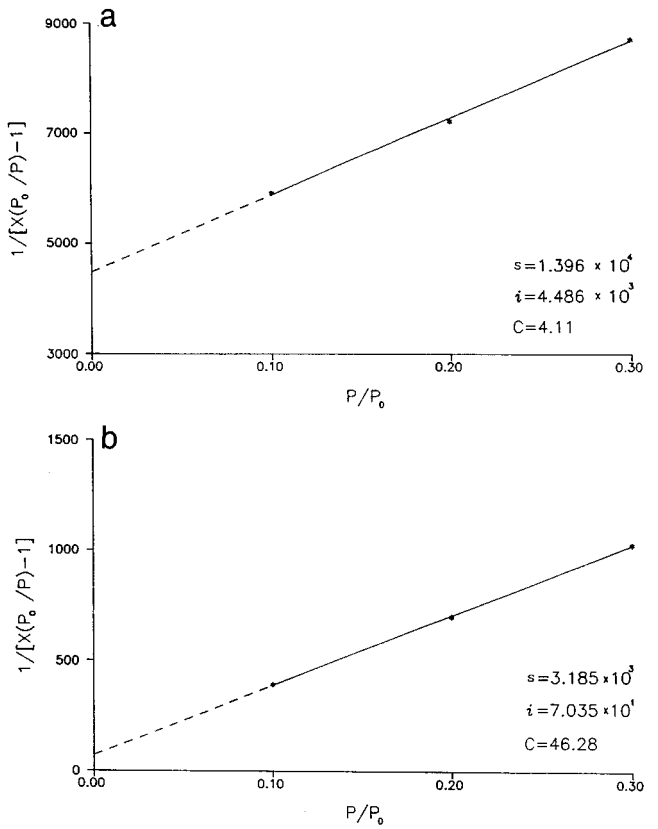

FIG. 4. BET plot of $LaNi_5$ (a) before activation and (b) after activation. s = slope, i = intercept, and C = BET constant.

volume of adsorbed or desorbed nitrogen at standard temperature and pressure per unit weight of the sample and P/P_0 is relative pressure.

Brunauer *et al.* (23), from an analysis of many adsorption isotherms, found that the adsorption isotherms correspond to one of five types. The adsorption isotherm of the activated $LaNi_5$ has a form that approaches type II among the five types. According to Brunauer *et al.*, type II is the isotherm very often observed when adsorption occurs on nonporous particles or on particles with pores larger than micropores (diameters of which are smaller than 15 Å).

TABLE 1
Specific Surface Areas, *S*, of $LaNi_5$ as a Function of the Number of Hydriding–Dehydriding Cycles, *n*

n	Specific surface area, *S*	
Before activation ($n = 0$)	0.04	
After activation	0–20 bar H_2, RT ($n = 11$) 0.27	0–8 bar H_2, RT ($n = 10$) 0.18
45		0.14
700		0.30
2530		0.39

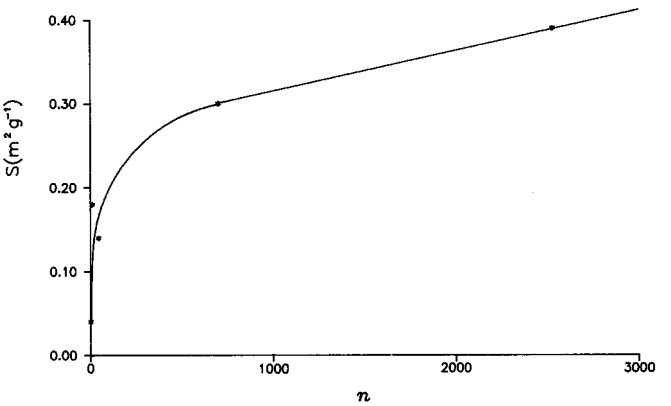

FIG. 5. Variation of the specific surface area, S, of $LaNi_5$ with the number of hydriding–dehydriding cycles, n, between zero and 8 bar H_2 at room temperature.

Above the relative pressure 0.3, de Boer (24) classified the hysteresis loops into five types according to pore shape. The hysteresis loop of activated $LaNi_5$ does not correspond to any of de Boer's five types. However, it is closer to type B as compared with the other types. The type B hysteresis loop is supposed to form when adsorption and desorption occur on the pore in the shape of a slit or on the interspace between parallel plates.

From the shapes of the adsorption isotherm and hysteresis loop it appears that the activated $LaNi_5$ particles are nonporous particles or particles with mesopores (diameter 15–1000 Å) or macropores (diameter >1000 Å).

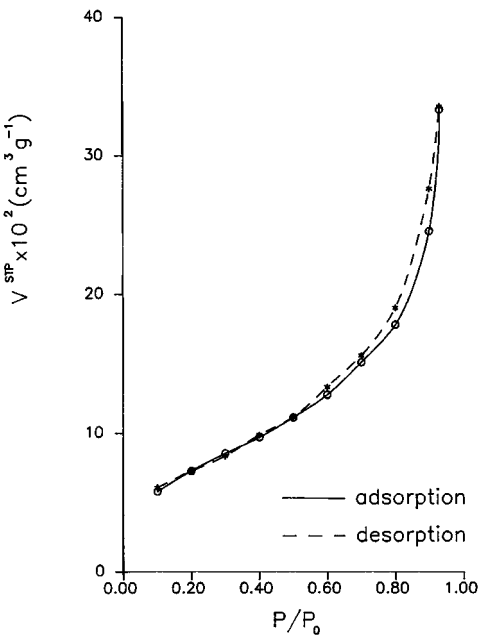

FIG. 6. Adsorption and desorption isotherms of activated $LaNi_5$.

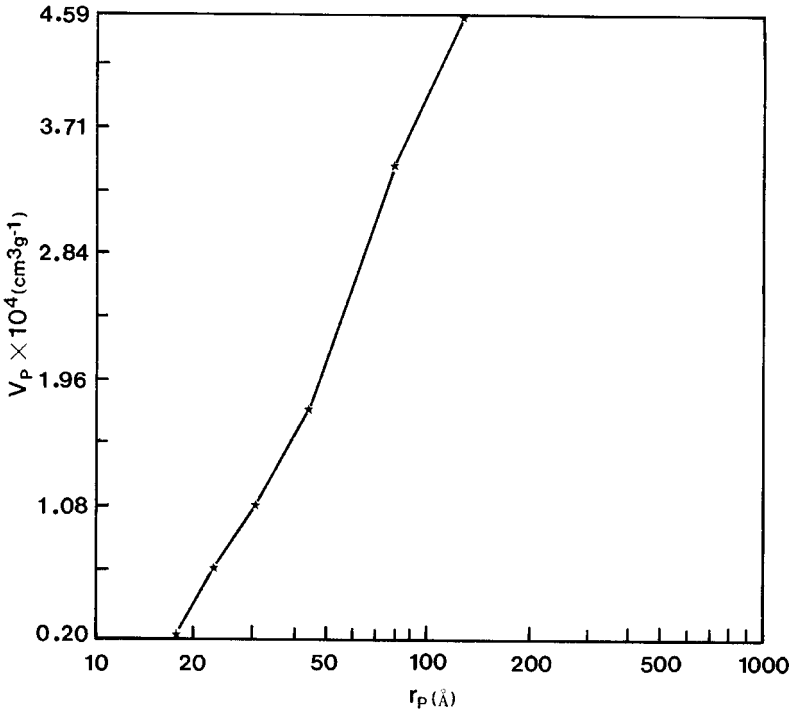

FIG. 7. Pore volume, V_p, versus pore radius, r_p, the cumulative pore volume plot of the activated $LaNi_5$.

As the saturated vapor pressure of the adsorbate decreases, the Gibbs free energy decreases. Since the relative pressure of the desorption isotherm is lower than that of the adsorption isotherm for the same quantity of adsorbate, the relative pressure of the desorption isotherm corresponds to a state of adsorbate more stable thermodynamically. Desorption is therefore used for the analysis of pore size distribution.

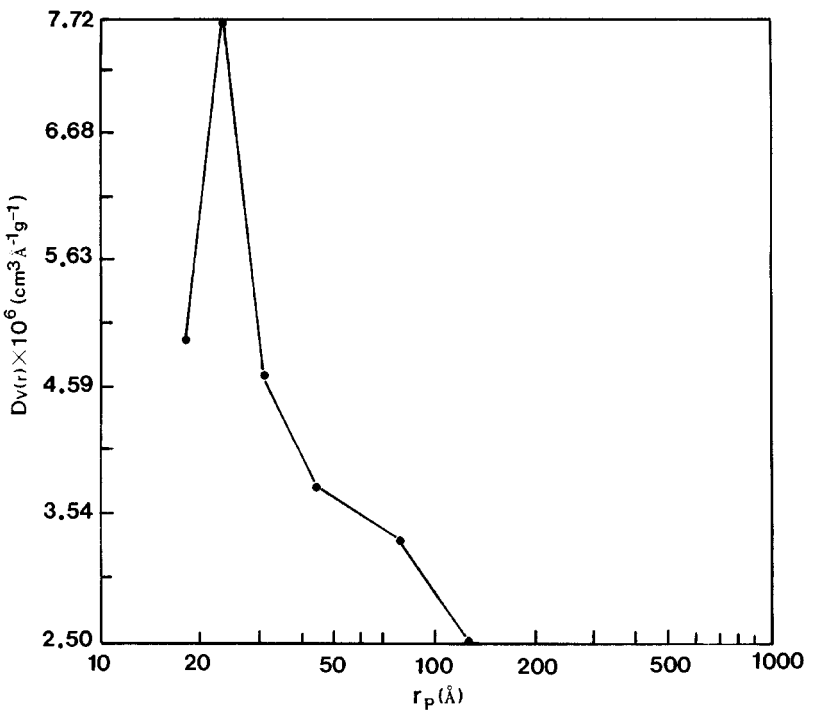

FIG. 8. Volume pore-size distribution function, $D_v(r)$, versus pore radius, r_p, the pore-size distribution curve of the activated $LaNi_5$.

When the pore is cylindrical, the Kelvin equation (20, p. 56) can be changed to the equation

$$\ln\frac{P}{P_0} = \frac{-2\gamma\bar{V}}{rRT}, \qquad [10]$$

where P is the equilibrium vapor pressure of liquid in the pore with diameter r, and P_0 the equilibrium vapor pressure of the same liquid on the plane surface. γ and $\bar{V}$ are the surface tension and molar volume of the liquid, respectively. Pore size analysis is carried out from the Eq. [10].

In Fig. 7 is a cumulative pore volume plot, a plot of pore volume, V_p, versus pore radius, r_p, of activated $LaNi_5$. Up to the relative pressure $P/P_0 = 0.93$, the total volume of the pore was $5.19 \times 10^{-4}\,cm^3\,g^{-1}$, which is very small, with a diameter smaller than 149.2 Å. This shows that the activated $LaNi_5$ has practically no pores.

Figure 8 is a pore-size distribution curve, a plot of the volume pore-size distribution function, $D_v(r)$, versus pore radius, r_p, of the activated $LaNi_5$. This curve shows that the sample contains mesopores with diameters of about 20–100 Å. The results in Figs. 7 and 8 show that activated

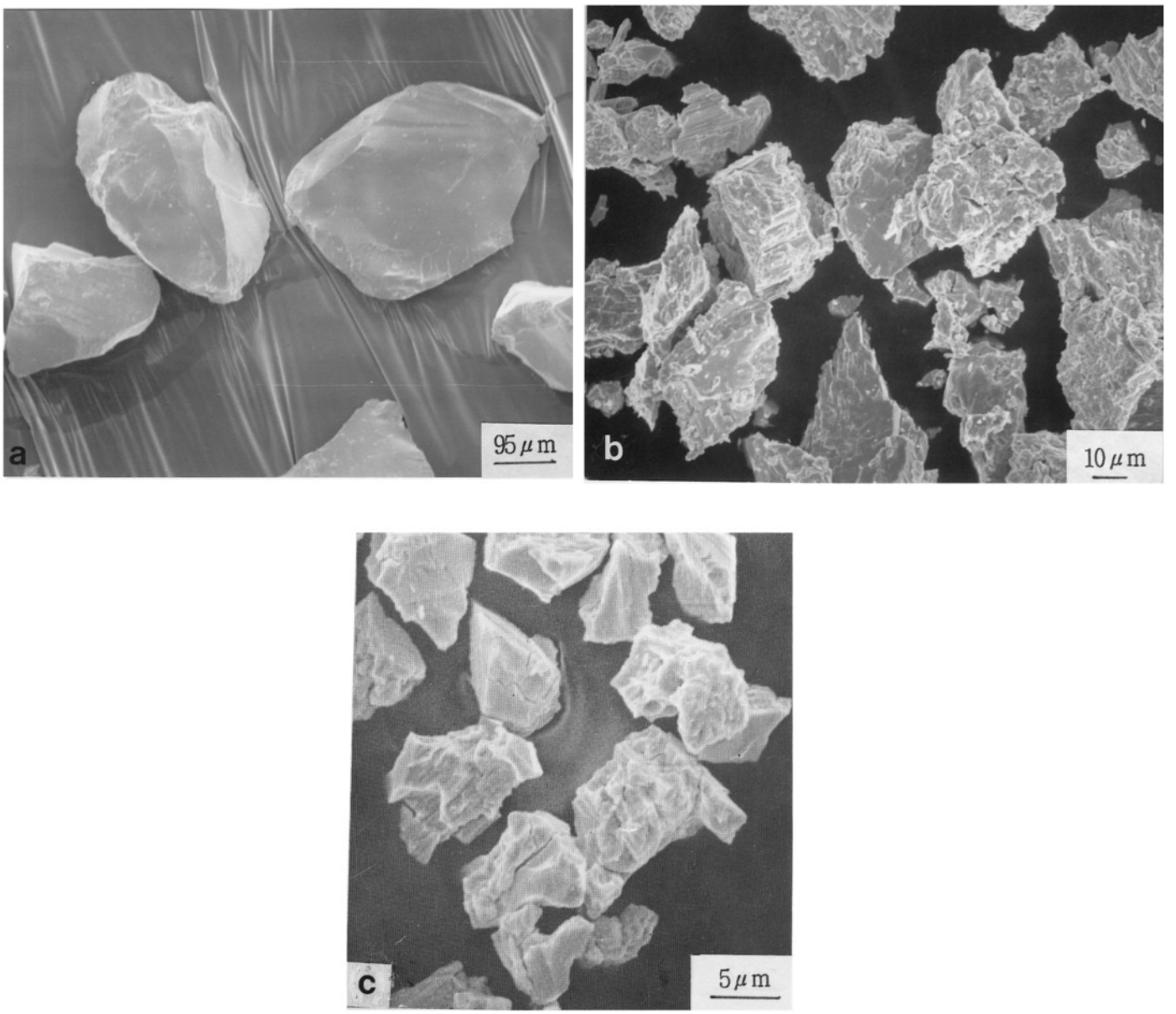

FIG. 9. Scanning electron micrographs of $LaNi_5$ (a) before activation (− 100 + 200 mesh), (b) after activation (11 hydriding–dehydriding cycles between 0 and 20 bar H_2 at 300 K), and (c) after 4400 hydriding–dehydriding cycles between 0 and 8 bar H_2 at 297 K.

$LaNi_5$ contains only a few pores with diameters around 20–110 Å.

Figure 9 is the scanning electron micrographs of $LaNi_5$ (a) before activation [−100 + 200 mesh (74–149 μm)] (b) after activation, and (c) after 4400 hydriding–dehydriding cycles between 0 and 8 bar H_2 at 297 K. The particles are finer after activation than before activation, and many cracks, which did not exist before activation, appeared in the particles. In addition, the particles were nonporous after activation (Fig. 9b). Figure 9c shows that the particles were still smaller and nonporous even after 4400 cycles.

Figure 10 shows the variation of the adsorption peak of activated $LaNi_5$ with N_2 mole fraction, x_{N_2}, in the gas mixture. For all x_{N_2} values, the first peak is considered as resulting from the thermal diffusion effect. The relatively sharp second peaks at $x_{N_2} = 0.10$–0.31 begin to broaden

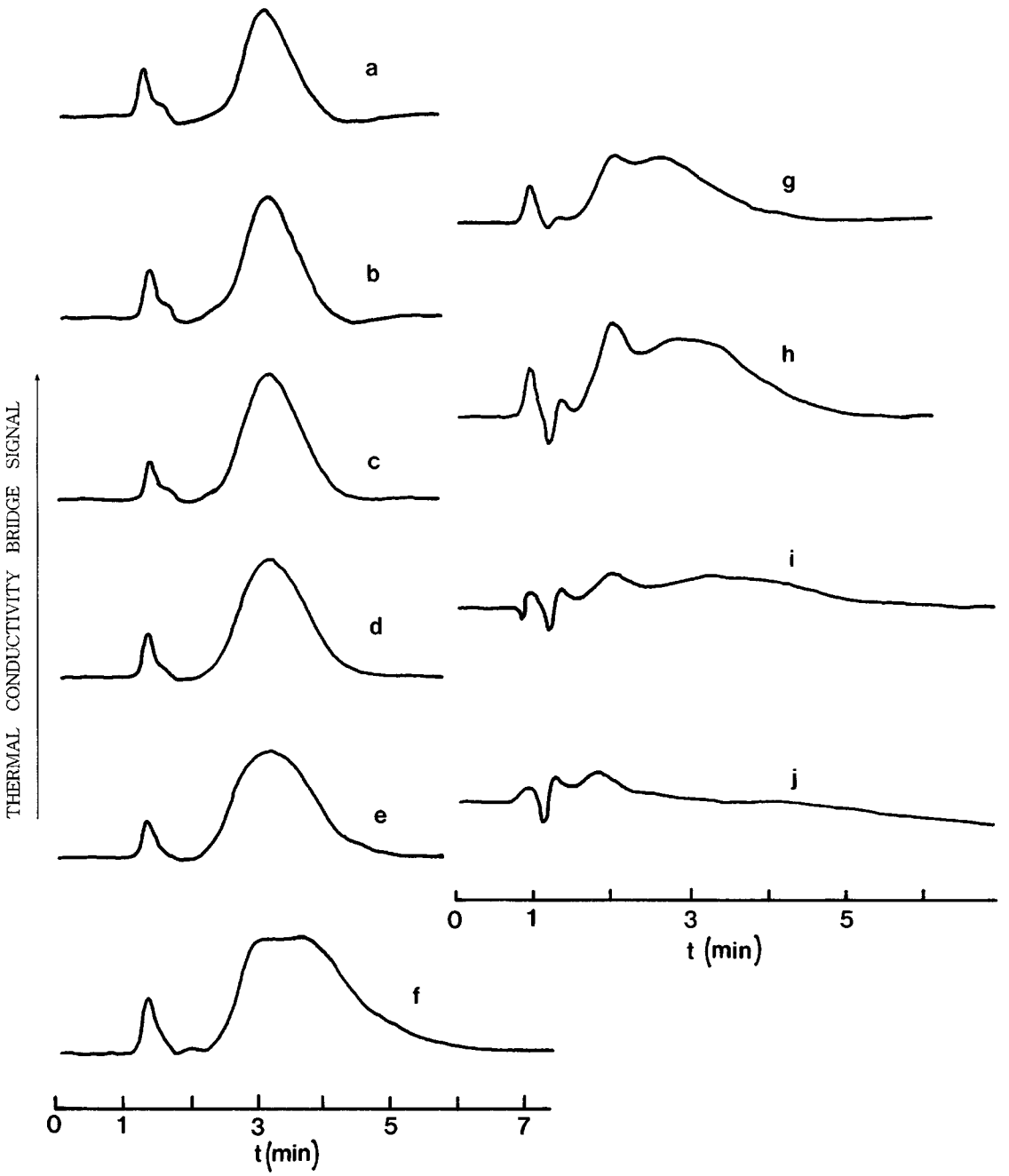

FIG. 10. Variation of the adsorption peak of the activated $LaNi_5$ with the N_2 mole fraction, x_{N_2}, in the gas mixture: (a) $x_{N_2} = 0.10$, (b) $x_{N_2} = 0.20$, (c) $x_{N_2} = 0.31$, (d) $x_{N_2} = 0.41$, (e) $x_{N_2} = 0.51$, (f) $x_{N_2} = 0.61$, (g) $x_{N_2} = 0.71$, (h) $x_{N_2} = 0.82$, (i) $x_{N_2} = 0.92$, and (j) $x_{N_2} = 0.95$.

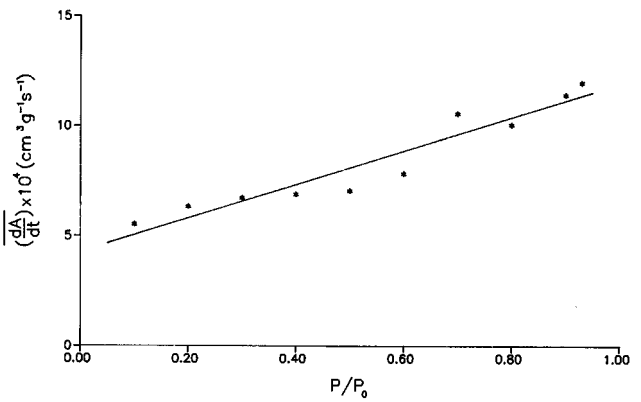

FIG. 11. Variation of the average adsorption rate, $(\overline{dA/dt})$, of the activated $LaNi_5$ with the relative pressure P/P_0.

a little from $x_{N_2} = 0.41$. From $x_{N_2} = 0.61$ the peaks begin to separate, and from $x_{N_2} = 0.71$ the peaks separate clearly.

We define the average adsorption rate $(\overline{dA}/\overline{dt})$ as the ratio of the quantity of adsorbed gas to the time for adsorption. Figure 11 gives the variation of the average adsorption rates of activated $LaNi_5$ with relative pressure P/P_0. The correlation coefficient was 0.96 and the linearity was not excellent. However, $(\overline{dA}/\overline{dt})$ is roughly proportional to P/P_0. According to the kinetic theory of gas, the adsorption rate is given as a linear function of gas pressure (25, 26). The result of this research shows that the adsorption rate of nitrogen on activated $LaNi_5$ is roughly proportional linearly to the gas pressure. As mentioned in the Introduction, Park and Lee (16) reported that the hydriding rates of $LaNi_5$ showed a first-order dependence on hydrogen pressure and that they are controlled by the hydrogen adsorption step on particle surfaces.

CONCLUSIONS

1. The specific surface area of activated $LaNi_5$ was $0.271 \pm 0.004\ m^2\ g^{-1}$. After activation, the specific surface area increased about seven times.

2. To reduce the effect of the increase in specific surface area with cycling, the kinetic data must be obtained and analyzed in a range of n as narrow as possible.

3. Adsorption and desorption isotherms of the activated $LaNi_5$ were obtained. The adsorption isotherm has a form that approaches type II among the five types of isotherms classified by Brunauer *et al.* (23). The hysteresis loop was similar to type B among de Boer's five types (24).

4. The results of analysis of the desorption pore-size distribution showed that activated $LaNi_5$ contained very few mesopores with diameters of about 20–110 Å.

5. The average nitrogen adsorption rate of activated $LaNi_5$ showed a first-order dependence on nitrogen pressure at 77 K.

ACKNOWLEDGMENT

The financial support of the Korean Science & Engineering Foundation (KOSEF, Serial No. 951–0806-028-1) is gratefully acknowledged.

REFERENCES

1. J. J. Reilly and R. H. Wiswall, *Inorg. Chem.* **13,** 218 (1974).
2. J. J. Reilly, *in* "Proceedings, International Symposium on Hydrides for Energy Storage, Geilo," p. 527. Pergamon, Oxford, 1977.
3. R. Wiswall, "Hydrogen in Metals II", Topics in Applied Physics, Vol. 29, 201 (1978).
4. M. Y. Song, J. K. Park, and J. Y. Lee, *J. Kor. Inst. Met.* **19,** 486 (1981).
5. O. Boser, *J. Less-Common Met.* **46,** 91 (1976).
6. P. D. Goodell and P. S. Rudman, *J. Less-Common Met.* **89,** 117 (1983).
7. J. J. Reilly and R. H. Wiswall, Jr., *Inorg. Chem.* **7,** 2254 (1968).
8. K. Nomura, E. Akiba, and S. Ono, *Int. J. Hydrogen Energ.* **6,** 295 (1981).
9 .M. Y. Song, M. Pezat, B. Darriet, and P. Hagenmuller, *J. Solid State Chem.* **56,** 191 (1985).
10. M. Y. Song, M. Pezat, B. Darriet, and P. Hagenmuller, *J. Mater. Sci.* **20,** 2958 (1985).
11. M. Y. Song, M. Pezat. B, Darriet, J. Y. Lee, and P. Hagenmuller, *J. Mater. Sci.* **21,** 346 (1986).
12. M. Y. Song, B. Darriet, M. Pezat, J. Y. Lee, and P. Hagenmuller, *J. Less-Common Met.* **118,** 235 (1986).
13. G. D. Sandrock, P. D. Goodell, E. L. Huston, and P. M. Golben, *in* "Proceedings, International Symposium on Metal Hydrogen Systems, Stuttgart, 1988."
14. A. Aoki, T. Yamamoto, Y. Satoh, K. Fukamich, and T. Masumoto, *Acta Metall.* **35,** 365 (1987).
15. M. Y. Song and H. R. Park, *J. Mater. Sci.* **27,** 1417 (1992).
16. C. N. Park and J. Y. Lee, *J. Less-Common Met.* **83,** 39 (1982).
17. J. de D. Lopez-Gonzales, F. G. Carpenter, and V. R. Deitz, *J. Res. Nat. Bur. Stand.* **55,** 11 (1955).
18. D. Kourilova and M. Krevel, *J. Chromatogr.* **65,** 71 (1972).
19. S. Lowell and S. Karp, *Anal. Chem.* **44,** 1706 (1972).
20. S. Lowell and J. E. Shields, "Powder Surface Area and Porosity," 2nd ed., p. 17. Chapman & Hall, London, 1984.
21. S. Tanaka, J. D. Clewley, and T. E. Flanagan, *J. Less-Common Met.* **56,** 137 (1977).
22. H. van Mal, *Philips Res. Rep. Suppl.*, 1 (1976).
23. S. Brunauer, L. S. Deming, W. S. Deming, and E. Teller, *J. Am. Chem. Soc.* **62,** 1723 (1940).
24. J. H. de Boer, "The Structure and Properties of Porous Materials," p. 68. Butterworth, London, 1958.
25. J. M. Thomas and W. J. Thomas, "Introduction to the Principles of Heterogeneous Catalysis," p. 34. Academic Press, London, 1967.
26. Gregg and Sing, "Adsorption, Surface Area and Porosity." Academic Press, London/New York, 1982.